Improving Synoptic and Intra-Seasonal Variability in CFSv2 via Stochastic Representation of Organized Convection

B. B. Goswami,[1] B. Khouider,[1] R. Phani,[2] P. Mukhopadhyay,[2] A. Majda,[3]

Corresponding author: B.B. Goswami, Department of Mathematics and Statistics, University of Victoria, Victoria, BC, Canada. (bgoswami@uvic.ca)

[1]Department of Mathematics and

To better represent organized convection in the Climate Forecast System version-2 (CFSv2), a stochastic multi-cloud model (SMCM) parameterization is adopted and a 15 year climate run is made. The last 10 years of simulations are analyzed here. While retaining an equally good mean state (if not better) as the parent model, the CFS-SMCM simulation shows significant improvement in the synoptic and intra-seasonal variability. The CFS-SMCM provides a better account of convectively coupled equatorial waves and the Madden-Julian oscillation (MJO). The CFS-SMCM exhibits improvements in northward and eastward propagation of intra-seasonal oscillation of convection including the MJO propagation beyond the maritime conti-

Statistics, University of Victoria, Victoria, BC, Canada.

[2]Indian Institute of Tropical Meteorology, Pune, India.

[3]Department of Mathematics and Center for Atmosphere and Ocean Sciences, Courant Institute for Mathematical Sciences, New York University, New York, NY, USA and Center for Prototype Climate Models, New York University Abu Dhabi, Abu Dhabi, United Arab Emirates

nent barrier, which is the Achilles Heal for coarse resolution GCMs. The distribution of precipitation events is better simulated in CFSsmcm and spreads naturally towards high precipitation events. Deterministic GCMs tend to simulate a narrow distribution with too much drizzling precipitation and too little high precipitation events.

1. Introduction

Tropical convection is comprised of clouds of different scales and is a manifestation of their interaction across scales [*Moncrieff et al.*, 2012]. Efforts to adequately represent these convective systems in a global climate model (GCM) has led the scientific community to think beyond conventional convective parameterization schemes (CCPS). Superparamaterized GCMs (SP-GCM) [*Grabowski*, 2001; *Khairoutdinov and Randall*, 2001] and global cloud resolving models (GCRM) [*Satoh et al.*, 2005] (also see *Randall* [2013] for a review) are such promising approaches. However, SP-GCMs and GCRMs are computationally expensive and definitely unlikely candidates for operational centers; especially for ensemble predictions. Nevertheless, the success of these approaches highlighted the importance of accurate representation of the sub-grid scale (SGS) variability collectively while realizing the individual behaviour of the convective elements, in the GCMs and their impact on the large-resolved scales.

The most common CCPS are based on the quasi-equilibrium assumption of *Arakawa and Schubert* [1974], the moist convective adjustment idea of *Manabe et al.* [1965], or the large-scale moisture convergence closure of *Kuo* [1965], and have deterministic closures which could only represent the ensemble mean, of the SGS convective heating. By adding stochastic flavour to these deterministic closures encouraging improvements have been observed [*Buizza et al.*, 2007; *Lin and Neelin*, 2003]. *Majda and Khouider* [2002] were the first to propose a stochastic model for convective inhibition (CIN) that allows both internal interactions between the convective elements and two-way interactions between the convective elements and the resolved scale. When coupled to a toy GCM, this stochastic parameterization produced eastward propagating convectively coupled waves that qualitatively resemble observations [*Khouider et al.*, 2003]. *Plant and Craig* [2008] derived a Poisson distribution for the number of plumes in a convective ensemble conditional on convective available potential energy (CAPE) and an exponentially distributed cloud base mass flux based on the theory of equilibrium statistical mechanics. Although not specifically designed for aggregating convection, its recent implementation in the NCAR atmospheric community model showed promising success [*Wang et al.*, 2016].

The stochastic multicloud model (SMCM) was first introduced in *Khouider et al.* [2010] to specifically capture the variability due to multi-scale organized convective systems in the spirit of the superparameterization approach, as a natural extension of the CIN stochastic model. By design, the stochastic multi-cloud model mimics the life cycle of organized tropical convective systems and its interaction with the large scales, as it is observed to involve three cloud types as the building block across multiple scales. It is based on a lattice particle interaction model for predefined microscopic (sub-grid) sites that make random transitions from one cloud type to another conditional to the large-scale state. In return the SMCM provides the cloud area fractions on the form of a Markov chain model which can be run in parallel with the climate model without any significant computational overhead. The SMCM was very successfully tested in both reduced-complexity tropical models and an aquaplanet global atmospheric model [*Frenkel et al.*, 2012, 2013; *Deng et al.*, 2015, 2016; *Ajayamohan et al.*, 2016] and also validated and calibrated using radar and large eddy simulation data [*Peters et al.*, 2013; *De La Chevrotière et al.*, 2015]. Here, we report, for the first time, the results of its implementation in the fully coupled CFSv2 model through the use of prescribed vertical profiles of heating and drying obtained from observations.

Comparison with observations show that the improvements in terms of synoptic and intra-seasonal variability are significant. In particular while CFSv2 exaggerates the intra-seasonal variance at the expense of the synoptic contribution, CFSsmcm shows a good balance between the two as in the observations.

2. Model Implementation and Setup

CFSv2 is the latest version of the NCEP climate forecast system [*Saha et al.*, 2014a]. While elaborate details on the SMCM and its GCM-implementation can be found in *Khouider et al.* [2010] and *Deng et al.* [2015] in particular, some changes had to be made to make it compatible with CFSv2. Some details on the implementation of the SMCM in CFS, using the CFS reanalysis [*Saha et al.*, 2010] climatology background to serve as a local radiative convective equilibrium (RCE), is given in the supplementary material. In a nutshell, moisture, temperature and boundary layer height are inputted from CFSv2 to the SMCM module. The convective heating rates for congestus, deep and stratiform (c/d/s) clouds are parameterized using the deviations of the thermo-dynamical/dynamical fields obtained from CFSv2, from the prescribed local RCE state. A stochastic lattice of 40x40 convective sites is overlaid over each GCM grid box, so that the sites are only a few kilometers apart in order to physically represent cloud type and at the same time capture the right amount of variability [*Frenkel et al.*, 2012]. An order parameter takes the values 0,1,2,3 at each lattice site according to whether the site is clear sky or occupied by c/d/s cloud, respectively. A single site transition occurs following a Markov jump stochastic process in the form of a multi-dimensional birth-death process whose transition probabilities depend explicitly on the large-scale mid-tropospheric dryness (MTD) and CAPE. The closure is formulated so that the c/d/s heating is proportional to the c/d/s cloud area fractions in a GCM grid. Deep convection is closed by combining CAPE and moisture adjustment processes while congestus heating is tied to low-level CAPE. Stratiform heating follows an adjustment equation towards a fraction of deep convection. The vertical distribution of heating and drying are based on imposed Q1 and Q2 profiles [*Johnson et al.*, 2016] carefully derived from reanalysis and TRMM data separately for each cloud type. In particular, congestus clouds heat the lower troposphere and cool the upper troposphere, deep convection heat the entire troposphere while stratiform clouds heat the upper troposphere and cool the lower troposphere. In this fashion the sequence of congestus, deep then stratiform cloud morphology following the progressive moistening and then drying of the lower troposphere yields a tilted heating field as it characterizes multi scale tropical convective systems [*Mapes et al.*, 2006; *Khouider and Majda*, 2006]. The sub-grid cloud-radiation interactions are not included.

The coupled CFS-SMCM model (CFSsmcm) is run for 15 years and the last 10 years were analyzed in comparison with a similar run using the original CFSv2 model as a control simulation. The two runs are made at T126 resolution and 10 minutes time step and validated against precipitation from TRMM3b42-v7 (0.25°x 0.25°; daily) [*Huffman et al.*, 2010], outgoing long-wave radiation (OLR) from NOAA (2.5°x 2.5°; daily) [*Liebmann and Smith*, 1996] and the thermo-dynamical and dynamical parameters from NCEP reanalysis [*Kalnay et al.*, 1996].

3. Results and Key Improvements

3.1. The mean state

Figure 1 provides an overall idea of the mean state (rainfall in shading and OLR contours) of the model. Precipitation is overestimated in both models, as evident from the average (over 50°S-50°N) annual mean precipitation shown by the numbers at the right hand top corners of the panels a-f. While the simulated climatologies look globally similar, region wise CFSsmcm shows a few improvements. For example, the dry biases over the Indian summer monsoon (ISM) region, northern Australia, and Amazonia and the wet bias over the western (especially during winter) and central-North Pacific have substantially reduced. Reduction of the wet bias over the equatorial Indian ocean during boreal summer is crucial as it has serious consequences in capturing interannual rainfall and sea surface temperature relationship. However some exaggeration in precipitation is noticeable west of the mountain ranges, namely Congo, Mekong and Andes, along the western coastlines. Figure S1 (in the supplemental material) provides details of differences of the simulated seasonal mean rainfall from the observations and the reference model. Precipitation biases are partly due to bias in local events and partly due to bias in the location of the inter-tropical convergence zone (ITCZ). Proper simulation of the ITCZ involves complex air-sea interactions which are beyond convective parameterization. So the overall annual rainfall mean state looks similar for the two simulations since they share the same ocean and air-sea interaction models. The double ITCZ problem remains particularly unresolved. The OLR contours are noted to follow the precipitation pattern. Noteworthy, in CFSsmcm the radiation feedback in the cloud scale has not been included. However, in CFSsmcm, like in reality [*Houze*, 1997], deep clouds decay through stratiform phase. This enables the radiation field sense and respond to the parameterized convective cloud. The fact that in the SMCM, the timescale of conversion of deep to stratiform is 25 minutes and that of decay of stratiform is 12 hours allows the persistence of a top heavy heating profile that forces convergence of moisture in the upper troposphere, which in turn allows the resolved scale micro-physics to produce stratus clouds and indirectly connect the cumulus parameterization to the radiation scheme and more importantly precipitation to the OLR field.

The boreal summer mean rainfall (in shading) and OLR (contours) is shown in Figure 1d-f. OLR contours are found to match the precipitation pattern closely. The annual-global-mean value suggests that, overall, CFSsmcm simulates a better OLR field. Indeed, an overestimation of both OLR and rainfall in CFSv2 simulations is associated with their biased joint-distribution as demonstrated in Section 3.4 along with the fact that CFSsmcm shows significant improvement in this regard. In the CFSsmcm climate, the improvement of OLR field over ISM region and south-east Pacific (off the coast of Peru) is noteworthy. Especially, in the backdrop of the fact that, a major concern of the CFSv2 simulations is the ISM dry bias [*Saha et al.*, 2014b].

One major concern of CFSv2 climate is an unrealistically cold middle troposphere [*Saha et al.*, 2014b] arguably due to the lack of proper stratiform cloud radiative forcing feedback [*Frenkel et al.*, 2015]. Figures 1g and 1h show the bias in the two simulated (zonally averaged) temperature fields. Apart from having cold bias in the mid-troposphere, CFSv2 has a warm bias in the top of the troposphere around 200-100hPa. CFSsmcm successfully gets rid of the warm bias at the top of the troposphere but shows limited ability to reduce the cold bias in the middle troposphere. As a testimony to simulating a better temperature field, CFSsmcm improves the circulation patterns (Figures not shown).

3.2. The variability

So far, CFSsmcm simulates a reasonable mean climate which is as good as CFSv2 climate, or better. Noteworthy, CFSv2 is already one of the best state-of-the-art GCMs [*Sabeerali et al.*, 2013]. Here we further assess CFSsmcm by analyzing the variability of the simulated climate. First, we examine the share of the synoptic variance (variance of 2-9 day Lanczos bandpass filtered rainfall anomalies) and the variance in the intra-seasonal oscillation (ISO) time-scale (variance of 10-90 day Lanczos bandpass filtered rainfall anomalies) in the total variability, following *Goswami et al.* [2014] who showed that CFSv2 systematically underestimates the contribution from synoptic variance.

Figure 2c reveals, the total boreal summer daily variance is over estimated in CFSsmcm simulations compared to that of TRMM (Figure 2a). CFSv2 simulations (Figure 2b) look better compared to CFSsmcm. Overestimation of the total daily variance suggests possible excessive simulation of extreme rainfall events by CFSsmcm. Which is, in fact, consistent with the results documented in Section 3.4. Based on our experience during the parameter tuning of the CFSsmcm, we posit that, a more careful calibration of the parameters responsible for MTD (though not considered here) would prove beneficial to get rid of this bias. Comparing Figures 2d & 2e and 2g & 2h, we note that CFSv2 underestimates (overestimates) the relative contribution of the synoptic (ISO) scale variance. This is consistent with the results of *Goswami et al.* [2014, 2015]. In the CFSsmcm simulations (Figures 2f and 2i), the relative contribution of the synoptic and ISO variances towards the total variance resembles much better with the observations. Interestingly, a similar improvement was seen in the superparameterized version of CFSv2 [*Goswami et al.*, 2015] as well. The unrealistic simulation of relative contributions of the synoptic and ISO variances resulting in a reasonable mean (Figure 1b and 1e) indicates the possibility of a wrong mechanism leading to a right result in CFSv2. This in fact reaffirms the importance of proper representation of the SGS scale variability in GCMs in order to better simulate the synoptic and intra-seasonal variability. For Figures 1d-i, it should be kept in mind that the percentage contributions are most relevant for the qualitative representation of organized convection dynamics than the total variance itself. The total variances are shown in see Figure S2.

3.3. Equatorial Wave Spectrum

Convectively coupled equatorial waves (CCEW) are the carriers of the perturbations occurring in the tropics. Accurate simulation of these waves is essential to simulate the climate variability. We carried out a wave number-frequency analysis following the methodology of *Wheeler and Kiladis* [1999] on OLR field for observation and the two simulations.

CFSv2 shows limited ability in capturing the CCEW spectrum. Apart from having realistic power in the n=1 equatorial Rossby (ER) waves, CFSv2 either overestimates or underestimates the CCEWs. The power in the Madden-Julien oscillation (MJO) is very weak with a slightly longer time-period than observations (Figure 3b). The power in the westward 3-6 day regime representing the tropical depressions is reasonable in the symmetric spectra of CFSv2 (Figure 3b); however it is overestimated in the antisymmetric spectra (Figure 3e).

Undoubtedly, the CCEW spectrum has improved significantly in CFSsmcm simulations (Figure 3c and 3f). The improvement of power in the MJO, n=-1 Kelvin, n=1 ER, n=1, 2 westward inertia-gravity (WIG) and n=0 mixed rossby-gravity (MRG) compared to the CFSv2 simulations is truly remarkable. However, CFSsmcm still needs to install some more power in the significant modes to match with the observations (Figure 3a and 3d). Also the power in the MJO has faster time periods in CFSsmcm than observations but the qualitatively improved WK-spectra suggests that CFSsmcm simulates better organization of convection.

3.4. Rainfall and OLR Distribution

A reasonable climatological mean rainfall (section 3.1) with a good organization of convection (section 3.3) suggests an improved simulation of mesoscale convective systems. This in turn suggests that, the CFSsmcm has an improved distribution of clouds associated with different rainfall events. Considering OLR as a proxy for cloud tops, we plot in Figure 4, the OLR-rainfall joint probability distribution.

In observations (Figures 4a and 4d), for ISM as well as for the entire tropics, we note OLR values roughly ranging between 100-300Wm^{-2}. The OLR values are centered about 200Wm^{-2} for the lowest intensity rainfall events which gets skewed toward relatively lower OLR values as we climb up the rainfall axis. Noticeably, OLR scatter for heavy rainfall is more in ISM than over tropics. This possibly is due to the fact that in the ISM climate, some of the highly rainy days are actually due to incessant rain coming from nimbostratus clouds rather than the result of a deep cumulonimbus convection [*Johnson and Houze*, 1987]. Also a feeble second maximum exists at about (270Wm^{-2}, 0-2 mmday^{-1}); more prominent for ISM climate. CFSv2 (Figure 4b and 4e) clearly misses to capture the wide spectrum of clouds over the entire tropics; ISM region being no exception. The majority of OLR values fall between 100-200 Wm^{-2} suggesting an affinity of CFSv2 for high level clouds. This may be a result of the simplified Arakawa-Schubert (SAS) convective scheme detraining only through the top of the cloud column resulting in a moist upper atmosphere and dry middle troposphere [*Pattanaik et al.*, 2013]. Improvement is evident in CFSsmcm simulation in Figure 4c and 4f. The OLR values are spread across a much wider range compared to CFSv2 simulations, although still narrower than observations, suggesting a better spectrum of clouds in the CFSsmcm atmosphere. Affinity to produce rain events with low associated OLR values is significantly reduced in the ISM domain and for the entire tropics as well. Noteworthy, CFSsmcm could capture the wider spread of OLR values associated with heavier rainfall events for ISM climate compared to the entire tropics. This suggests the ability of CFSsmcm to recognize the complexity of the ISM climate and to distinguish it from the rest of the tropics. The secondary peak at about 270Wm^{-2} is also captured, although exaggerated. This improved simulation of the rainfall-cloud association suggests a better simulation of mesoscale complexes in CFSsmcm, which in turn promises a better organization and variability in the simulated climate.

3.5. Organization and Propagation Features

The organization of convection over the tropics is relevant only when it propagates in the right direction. On the intra-seasonal scales, convection is observed to oscillate quasiperiodically with periodicity 30-60 days northward in the ISM region and eastward along the tropical channel, especially over the warm waters of Indian Ocean and West Pacific during both boreal summer and winter [*Goswami*, 2012]. In Figure 5 we plotted the lag-regressed 20-90 day band-pass filtered rainfall and zonal wind at 850hPa. In Figure 5a-c, the rain and wind fields are averaged for 70°E-90°E and for Figure 5d-i, they are averaged over 5°S-5°N.

In the observations (Figure 5a) the convection starts at the equator and moves to about 20°N with a phase speed of approximately a degree a day. There are two maxima of convection, one over the warm waters of the equatorial Indian Ocean (EIO) and the other over the monsoon trough, between 15°N-20°N. The two associated maxima in the regressed zonal winds suggests the dynamically coupled nature of organized convection. CFSv2 (Figure 5b) captures this feature reasonably well although the migration is not as smooth as in observations with a hint of southward movement 2-3 degrees north of the equator. This southward movement of convection is restricted to the south of the equator in observations (Figure 5a). Convection over the EIO is overestimated, which *Goswami et al.* [2014] had attributed to unrealistic air-sea coupling in CFSv2. Moreover, the inability to simulate the second maximum in the regressed zonal winds raises questions on CFSv2's ability to simulate the coupled nature of tropical convection. In CFSsmcm simulation (Figure 5c), the northward propagation of convection is as prominent as in the CFSv2 and is quantitatively closer to the observed phase speed unlike CFSv2 which appears to be slower. Like in CFSv2, the southward migration of convection starts from north of the equator in CFSsmcm as well. In addition, the maximum in convection over

Indian Ocean is seen south of the equator at approximately 5°S. However, the tendency to simulate two maxima for the regressed zonal winds suggest improvement in the circulation associated with the convection in the CFSsmcm simulated ISM.

Figure 5d-f and 5g-i show the eastward propagation of convection during boreal summer and winter respectively. Clear eastward movement is observed (Fig 5d and 5g) in both seasons starting from central-EIO to west-central Pacific with a relatively weaker organization over the Maritime Continent. This is possibly due to the competition between the strong diurnal cycle of convection and eastward moving organized convection to kill each other over the Maritime continent [*Oh et al.*, 2013]. Noteworthy, although obvious, convection over the EIO (west-central Pacific) is relatively stronger (weaker) in the boreal winter than in summer. In CFSv2 simulations (Figure 5e and 5h), convection weakens once it reaches Maritime Continent and do not revive passed this barrier, unlike observations. The relatively stronger convection over the east-EIO in winter than in summer is captured to some extent. However, in winter the propagation features are simulated even worse and appear to be almost like a stationary convection over 90°E. In CFSsmcm simulations (Figure 5f and 5i), the eastward propagation is much better and more prominent than in CFSv2. The major features, like, the revival of convection passed the Maritime Continent and the relative strengths of convection in the boreal summer and winter over the Indian Ocean and the west-central Pacific are reasonably well captured. However the phase speed appears to be faster than observations and the propagation looks very wobbly. This wobbliness, although maybe is exaggerated by an excessive stochastic variability, is arguably due to the chaotic nature of synoptic and mesoscale convective events embedded in the MJO envelope. The propagation of individual synoptic and intra-seasonal events is also better simulated by CFSsmcm as more intermittent convective systems are seen in both time and space (results not shown).

4. Conclusion and Discussions

The SMCM, which was designed to better represent the unresolved variability associated with multiscale organized convective systems in GCMs, is implemented in CFSv2. A first-hand look at the mean state and the variability of the CFSsmcm 10-years climate is reported here. While the mean state of CFSsmcm is comparable to that of CFSv2, there are some minor improvements. One of the minor improvements include reduction of the dry bias in the ISM seasonal rainfall, which is of major importance. The most significant improvements are noted in the synoptic and intra-seasonal scale. The CCEWs are better simulated in CFSsmcm. The simulated OLR (read cloud) look more realistic in CFSsmcm spanning across low-middle-high values like the observations. The organization of convection and its propagation features are much improved compared to CFSv2. The model also shows better ability, than CFSv2, to identify and distinguish ISM climate from the rest of the tropics through simulation of rainfall-OLR relation. All the improvements shown by CFSsmcm relative to CFSv2 are significant because of two major reasons: first, CFSv2 is already one of the best available state-of-the-art climate models, and second, the improvements have come without any extra computational cost than running the conventional CFSv2 model. This is why CFSsmcm can be considered as a successful attempt to break the convective parameterization deadlock.

During the development of the CFSsmcm model, we noted some interesting behaviour. The model's overall performance show high sensitivity to the mid tropospheric dryness (MTD) parameter. The simulation of MJO gets highly affected (as we noticed by plotting WK spectra) by changing MTD. Another parameter affecting MJO simulation is the lifetime of stratiform clouds. We are planning a few more test runs to study the models sensitivity to MTD. We believe that the excessive overall variance can be alleviated through a more careful calibration of the MTD parameter. In particular, a different MTD value may be used over land and over ocean as convection responds differently over land and ocean. Noteworthy, realistic simulation of eastward propagating Kelvin waves is a consistent feature of the model, even in its beta version.

We are extending our analyses further to get more insight of CFSsmcm behaviour in particular and the issue of convective parameterization in general. Primarily we would like to investigate the simulation of convectively coupled equatorial waves in the CFSsmcm. Also interactive radiation at the sub-grid scale will be considered following the work of *Frenkel et al.* [2015]. The fact that SMCM is built on a robust mathematical framework, makes model improvements more transparent. This, in turn, makes the process of model development more of an outcome of a systematic analysis then being a serendipity [*Held*, 2005] .

Acknowledgments. The research of BK is partially funded by a grant from the Government of India through the National Monsoon Mission (NMM) and a discovery grant from the Canadian Natural and Sciences and Engineering Research Council. BBG is a post doctoral fellow through BK's NMM grant. TRMM3b42-v7 data is obtained from *http* :

//disc.gsfc.nasa.gov/datacollection/TRMM_3B42_Daily_7.html. NOAA OLR data is obtained from *ftp : //ftp.cdc.noaa.gov/Datasets/interp*$_O$*LR/olr.day.mean.nc*. The NCEP reanalyses product is obtained from *http : //www.esrl.noaa.gov/psd/data/gridded/data.ncep.reana* CFSR data for constructing the background for SMCM is obtained from *http : //rda.ucar.edu/datasets/ds*093.2/.

References

Ajayamohan, R. S., B. Khouider, A. J. Majda, and Q. Deng (2016), Role of stratiform heating on the organization of convection over the monsoon trough, *Clim. Dyn.*, pp. 1–20, doi:10.1007/s00382-016-3033-7.

Arakawa, A., and W. H. Schubert (1974), Interaction of a Cumulus Cloud Ensemble with the Large-Scale Environment, Part I, *J. Atmos. Sci.*, *31*(3), 674–701, doi:10.1175/1520-0469(1974)031<0674:IOACCE>2.0.CO;2.

Buizza, R., M. Miller, and T. N. Palmer (2007), Stochastic representation of model uncertainties in the ECMWF ensemble prediction system, *Q. J. R. Meteorol. Soc.*, *125*(560), 2887–2908, doi:10.1002/qj.49712556006.

De La Chevrotière, M., Michèle, B. Khouider, and A. Majda (2015), Stochasticity of convection in giga-les data, *Clim. Dyn.*, *47*(5), 1845–1861, doi:10.1007/s00382-015-2936-z.

Deng, Q., B. Khouider, and A. J. Majda (2015), The MJO in a Coarse-Resolution GCM with a Stochastic Multicloud Parameterization, *J. Atmos. Sci.*, *72*(1), 55–74, doi:10.1175/JAS-D-14-0120.1.

Deng, Q., B. Khouider, A. J. Majda, and R. S. Ajayamohan (2016), Effect of Stratiform Heating on the Planetary-Scale Organization of Tropical Convection, *J. Atmos. Sci.*, *73*(1), 371–392, doi:10.1175/JAS-D-15-0178.1.

Frenkel, Y., A. J. Majda, and B. Khouider (2012), Using the Stochastic Multicloud Model to Improve Tropical Convective Parameterization: A Paradigm Example, *J. Atmos. Sci.*, *69*(3), 1080–1105, doi:10.1175/JAS-D-11-0148.1.

Frenkel, Y., A. J. Majda, and B. Khouider (2013), Stochastic and deterministic multicloud parameterizations for tropical convection, *Clim. Dyn.*, *41*(5-6), 1527–1551, doi:10.1007/s00382-013-1678-z.

Frenkel, Y., A. J. Majda, and S. N. Stechmann (2015), Cloud-radiation feedback and atmosphere-ocean coupling in a stochastic multicloud model, *Dynamics of Atmospheres and Oceans*, *71*, 35 – 55, doi:10.1016/j.dynatmoce.2015.05.003.

Goswami, B. B., M. Deshpande, P. Mukhopadhyay, S. K. Saha, S. A. Rao, R. Murthugudde, and B. N. Goswami (2014), Simulation of monsoon intraseasonal variability in NCEP CFSv2 and its role on systematic bias, *Clim. Dyn.*, *43*(9-10), 2725–2745, doi:10.1007/s00382-014-2089-5.

Goswami, B. B., R. P. M. Krishna, P. Mukhopadhyay, M. Khairoutdinov, and B. N. Goswami (2015), Simulation of the Indian Summer Monsoon in the Superparameterized Climate Forecast System Version 2: Preliminary Results, *J. Clim.*, *28*(22), 8988–9012, doi:10.1175/JCLI-D-14-00607.1.

Goswami, B. N. (2012), South Asian Monsoon, in *South Asian monsoon*, edited by W. K.-M. Lau and D. E. Waliser, chap. 2, pp. 21–72, Springer Berlin Heidelberg, Berlin, Heidelberg, doi:10.1007/978-3-642-13914-7_2.

Grabowski, W. W. (2001), Coupling Cloud Processes with the Large-Scale Dynamics Using the Cloud-Resolving Convection Parameterization (CRCP), *J. Atmos. Sci.*, *58*(9), 978–997, doi:10.1175/1520-0469(2001)058<0978:CCPWTL>2.0.CO;2.

Held, I. M. (2005), The gap between simulation and understanding in climate modeling, *Bulletin of the American Meteorological Society*, *86*(11), 1609–1614, doi:10.1175/BAMS-86-11-1609.

Houze, R. A. (1997), Stratiform precipitation in regions of convection: A meteorological paradox?, *Bulletin of the American Meteorological Society*, *78*(10), 2179–2196, doi:10.1175/1520-0477(1997)078<2179:SPIROC>2.0.CO;2.

Huffman, G. J., R. F. Adler, D. T. Bolvin, and E. J. Nelkin (2010), The TRMM Multi-satellite Precipitation Analysis (TMPA), in *Satellite Rainfall Applications for Surface Hydrology*, pp. 3–22, Springer, doi:10.1007/978-90-481-2915-7_1.

Johnson, R., and R. J. Houze (1987), Precipitating cloud systems of the Asian monsoon, in *Monsoon Meteorology*, edited by C.-P. Chang and T. Krishnamurti, chap. 10, pp. 298–353, Oxford University Press.

Johnson, R. H., P. E. Ciesielski, and T. M. Rickenbach (2016), A Further Look at Q1 and Q2 from TOGA COARE, *Meteor. Monogr.*, *56*, 1.1–1.12, doi:10.1175/AMSMONOGRAPHS-D-15-0002.1.

Kalnay, E., M. Kanamitsu, R. Kistler, W. Collins, D. Deaven, L. Gandin, M. Iredell, S. Saha, G. White, J. Woollen, Y. Zhu, A. Leetmaa, R. Reynolds, M. Chelliah, W. Ebisuzaki, W. Higgins, J. Janowiak, K. C. Mo, C. Ropelewski, J. Wang, R. Jenne, and D. Joseph (1996), The NCEP/NCAR 40-Year Reanalysis Project, *Bull. Am. Meteorol. Soc.*, *77*(3), 437–471, doi:10.1175/1520-0477(1996)077<0437:TNYRP>2.0.CO;2.

Khairoutdinov, M. F., and D. A. Randall (2001), A cloud resolving model as a cloud parameterization in the NCAR Community Climate System Model: Preliminary results, *Geophys. Res. Lett.*, *28*(18), 3617–3620, doi:10.1029/2001GL013552.

Khouider, B., and A. J. Majda (2006), A simple multicloud parameterization for convectively coupled tropical waves. part i: Linear analysis, *Journal of the Atmospheric Sciences*, *63*(4), 1308–1323, doi:10.1175/JAS3677.1.

Khouider, B., A. J. Majda, and M. A. Katsoulakis (2003), Coarse-grained stochastic models for tropical convection and climate., *Proc. Natl. Acad. Sci. U.S.A.*, *100*(21), 11,941–6, doi:10.1073/pnas.1634951100.

Khouider, B., J. Biello, and A. J. Majda (2010), A stochastic multicloud model for tropical convection, *Commun. Math. Sci.*, *8*(1), 187–216.

Kuo, H. L. (1965), On Formation and Intensification of Tropical Cyclones Through Latent Heat Release by Cumulus Convection, *J. Atmos. Sci.*, *22*(1), 40–63, doi:10.1175/1520-0469(1965)022<0040:OFAIOT>2.0.CO;2.

Liebmann, B., and C. Smith (1996), Description of a Complete (Interpolated) Outgoing Longwave Radiation Dataset., *Bull. Am. Meteorol. Soc.*, *77*, 1275–1277.

Lin, J. W.-B., and J. D. Neelin (2003), Toward stochastic deep convective parameterization in general circulation models, *Geophys. Res. Lett.*, *30*(4), doi:10.1029/2002GL016203.

Majda, A. J., and B. Khouider (2002), Stochastic and mesoscopic models for tropical convection, *Proc. Natl. Acad. Sci. U.S.A.*, *99*(3), 1123–1128, doi:10.1073/pnas.032663199.

Manabe, S., J. Smagorinsky, and R. F. Strikler (1965), Simulated climatology of a general circulation model with a hydrologic cycle, *Mon. Weather Rev.*, *93*(12), 769–798, doi: 10.1175/1520-0493(1965)093<0769:SCOAGC>2.3.CO;2.

Mapes, B., S. Tulich, J. Lin, and P. Zuidema (2006), The mesoscale convection life cycle: Building block or prototype for large-scale tropical waves?, *Dyn. Atmos. Oceans*, *42*(1-4), 3–29, doi:10.1016/j.dynatmoce.2006.03.003.

Moncrieff, M., D. Waliser, M. J. Miller, M. A. Shapiro, G. R. Asrar, and J. Caughey (2012), Multiscale convective organization and the YOTC virtual global field campaign, *Bull. Am. Meteorol. Soc.*, *93*(8), 1171–1187.

Oh, J.-H., B.-M. Kim, K.-Y. Kim, H.-J. Song, and G.-H. Lim (2013), The impact of the diurnal cycle on the MJO over the Maritime Continent: a modeling study assimilating TRMM rain rate into global analysis, *Clim. Dyn.*, *40*(3-4), 893–911, doi:10.1007/s00382-012-1419-8.

Pattanaik, S., S. Abhilash, S. De, A. K. Sahai, R. Phani, and B. N. Goswami (2013), Influence of convective parameterization on the systematic errors of Climate Forecast System (CFS) model over the Indian monsoon region from an extended range forecast perspective, *Clim. Dyn.*, *41*(2), 341–365, doi:10.1007/s00382-013-1662-7.

Peters, K., C. Jakob, L. Davies, B. Khouider, and A. J. Majda (2013), Stochastic Behavior of Tropical Convection in Observations and a Multicloud Model, *J. Atmos. Sci.*, *70*(11), 3556–3575, doi:10.1175/JAS-D-13-031.1.

Plant, R. S., and G. C. Craig (2008), A stochastic parameterization for deep convection based on equilibrium statistics, *J. Atmos. Sci.*, *65*, 87?105, doi: doi:10.1175/2007JAS2263.1.

Randall, D. A. (2013), Beyond deadlock, *Geophys. Res. Lett.*, *40*(22), 5970–5976, doi: 10.1002/2013GL057998.

Sabeerali, C. T., A. Ramu Dandi, A. Dhakate, K. Salunke, S. Mahapatra, and S. A. Rao (2013), Simulation of boreal summer intraseasonal oscillations in the latest CMIP5 coupled GCMs, *J. Geophys. Res. Atmos.*, *118*(10), 4401–4420, doi:10.1002/jgrd.50403.

Saha, S., S. Moorthi, H.-L. Pan, X. Wu, J. Wang, S. Nadiga, P. Tripp, R. Kistler, J. Woollen, D. Behringer, H. Liu, D. Stokes, R. Grumbine, G. Gayno, J. Wang, Y.-T. Hou, H.-Y. Chuang, H.-M. H. Juang, J. Sela, M. Iredell, R. Treadon, D. Kleist, P. Van Delst, D. Keyser, J. Derber, M. Ek, J. Meng, H. Wei, R. Yang, S. Lord, H. Van Den Dool, A. Kumar, W. Wang, C. Long, M. Chelliah, Y. Xue, B. Huang, J.-K. Schemm, W. Ebisuzaki, R. Lin, P. Xie, M. Chen, S. Zhou, W. Higgins, C.-Z. Zou, Q. Liu, Y. Chen, Y. Han, L. Cucurull, R. W. Reynolds, G. Rutledge, and M. Goldberg (2010), The NCEP Climate Forecast System Reanalysis, *Bull. Am. Meteorol. Soc.*, *91*(8), 1015–1057, doi:10.1175/2010BAMS3001.1.

Saha, S., S. Moorthi, X. Wu, J. Wang, S. Nadiga, P. Tripp, D. Behringer, Y.-T. Hou, H.-y. Chuang, M. Iredell, M. Ek, J. Meng, R. Yang, M. P. Mendez, H. van den Dool, Q. Zhang, W. Wang, M. Chen, and E. Becker (2014a), The NCEP Climate Forecast System Version 2, *J. Clim.*, *27*(6), 2185–2208, doi:10.1175/JCLI-D-12-00823.1.

Saha, S. K., S. Pokhrel, H. S. Chaudhari, A. Dhakate, S. Shewale, C. T. Sabeerali, K. Salunke, A. Hazra, S. Mahapatra, and A. S. Rao (2014b), Improved simulation of indian summer monsoon in latest ncep climate forecast system free run, *Int. J. Clim.*, *34*(5), 1628–1641, doi:10.1002/joc.3791.

Satoh, M., H. Tomita, H. Miura, S. Iga, and T. Nasuno (2005), Development of a global cloud resolving model a multi-scale structure of tropical convections, *J. Earth Simulator*, *3*(September), 11–19.

Wang, Y., G. J. Zhang, and G. C. Craig (2016), Stochastic convective parameterization improving the simulation of tropical precipitation variability in the ncar cam5, *Geophys. Res. Lett.*, *43*(12), 6612–6619, doi:10.1002/2016GL069818, 2016GL069818.

Wheeler, M., and G. N. Kiladis (1999), Convectively Coupled Equatorial Waves: Analysis of Clouds and Temperature in the Wavenumber-Frequency Domain, *J. Atmos. Sci.*, *56*(3), 374–399, doi:10.1175/1520-0469(1999)056<0374:CCEWAO>2.0.CO;2.

Figure 1. Climatological annual mean rainfall (shaded) and OLR (contours) (a)TRMM and NOAA, (b)CFSv2 and (c)CFSsmcm. Climatological boreal summer mean Rainfall (shaded) and OLR (contours) (d)TRMM and NOAA, (e)CFSv2 and (f)CFSsmcm. [OLR contour interval is $20Wm^{-2}$; $240Wm^{-2}$ contour is labeled for reference]. Climatological annual zonal mean temperature bias wrt NCEP reanalysis (g)CFSv2 and (h)CFSsmcm. The global mean annual rainfall values are shown at the right hand top corner of the panels (a) to (c) and the global mean boreal summer OLR values are shown at the right hand top corner of the panels (d) to (f).

Figure 2. Boreal summer total daily rainfall variance (mm^2day^{-2}) (a)TRMM, (b)CFSv2 and (c)CFSsmcm. Contribution of synoptic variance to the total (d)TRMM, (e)CFSv2 and (f)CFSsmcm. Contribution of ISO variance to the total (g)TRMM, (h)CFSv2 and (i)CFSsmcm.

Figure 3. Wheeler-Kiladis spectra of OLR from (a)NOAA, (b)CFSv2 and (c)CFSsmcm, for the symmetric component. The corresponding anti-symmetric spectra are shown in panels d, e and f, respectively.

Figure 4. Joint distribution (in %) of OLR-rainfall over ISM region (15°S-30°N, 50°E-110°E), during boreal summer, for (a)Observation (TRMM-NOAA), (b)CFSv2 and (c)CFSsmcm. The corresponding distribution for over entire tropics (30°S-30°N) for the whole year is shown in panels d, e and f, respectively. [NOTE: TRMM data is regridded to 2.5°x 2.5°resolution to plot this figure.]

Figure 5. Lag-regressed 20-90 day band-pass filtered rainfall (shaded) and zonal wind at 850hPa (contours). In Figure 5a-c, the regressed rain and wind are averaged for 70°E-90°E. For Figure 5d-i, the regressed fields are averaged over 5°S-5°N.

Figure 1.

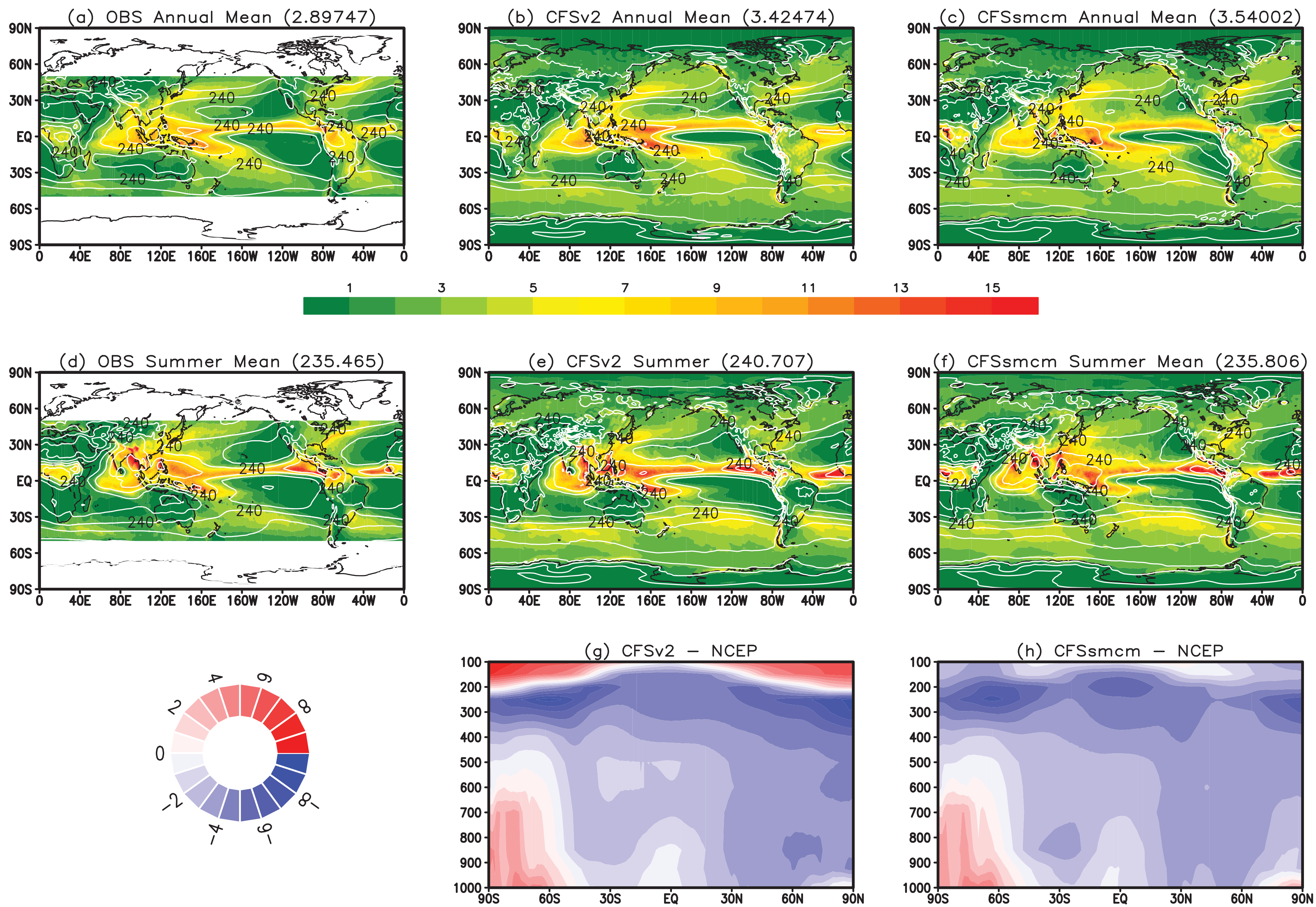

(a) OBS Annual Mean (2.89747)
(b) CFSv2 Annual Mean (3.42474)
(c) CFSsmcm Annual Mean (3.54002)
(d) OBS Summer Mean (235.465)
(e) CFSv2 Summer (240.707)
(f) CFSsmcm Summer Mean (235.806)
(g) CFSv2 – NCEP
(h) CFSsmcm – NCEP

Figure 2.

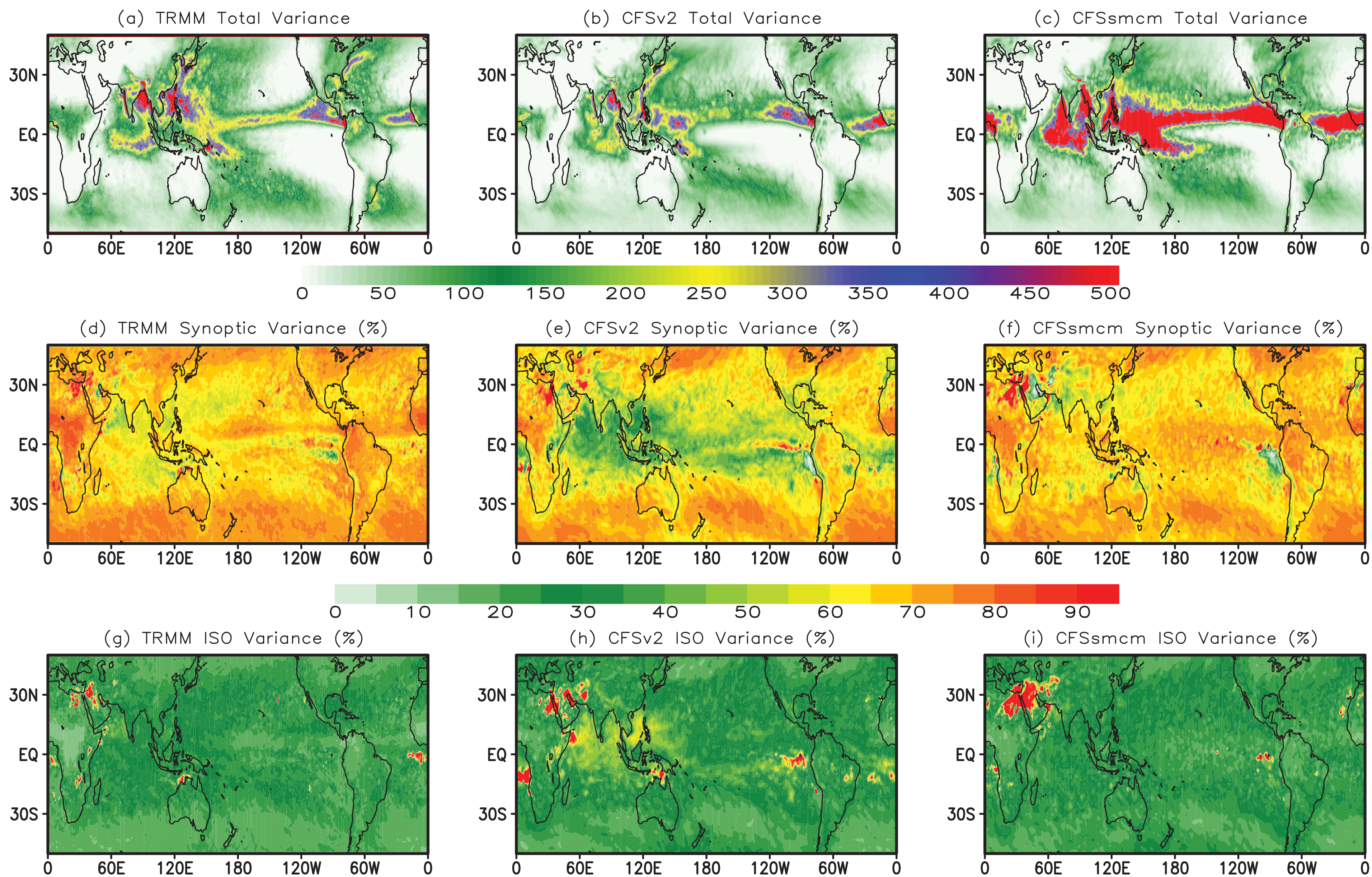

(a) TRMM Total Variance
(b) CFSv2 Total Variance
(c) CFSsmcm Total Variance
0 50 100 150 200 250 300 350 400 450 500
(d) TRMM Synoptic Variance (%)
(e) CFSv2 Synoptic Variance (%)
(f) CFSsmcm Synoptic Variance (%)
0 10 20 30 40 50 60 70 80 90
(g) TRMM ISO Variance (%)
(h) CFSv2 ISO Variance (%)
(i) CFSsmcm ISO Variance (%)
30N
EQ
30S
0 60E 120E 180 120W 60W 0

Figure 3.

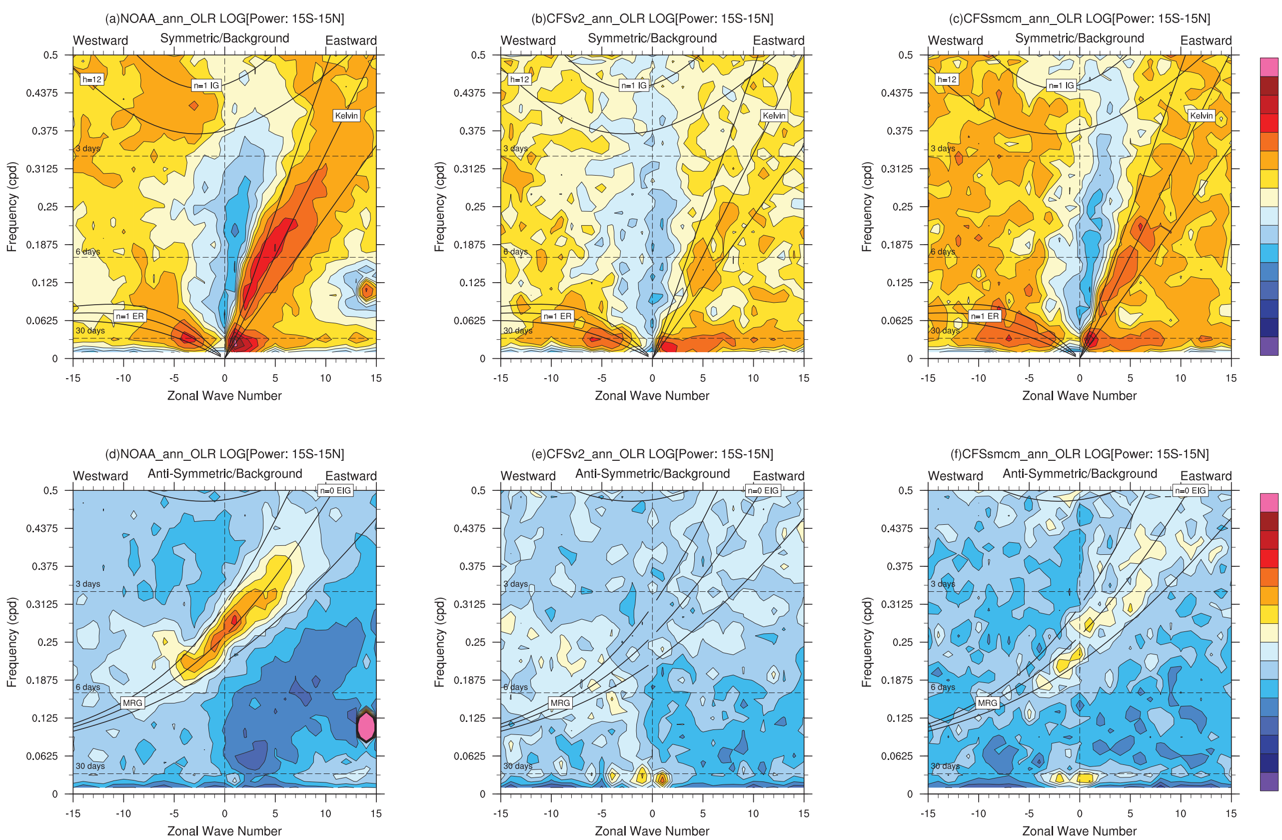

(a)NOAA_ann_OLR LOG[Power: 15S-15N]
(b)CFSv2_ann_OLR LOG[Power: 15S-15N]
(c)CFSmcm_ann_OLR LOG[Power: 15S-15N]
Westward
Symmetric/Background
Eastward
h=12
n=1 IG
Kelvin
n=1 ER
3 days
6 days
30 days
Frequency (cpd)
Zonal Wave Number
(d)NOAA_ann_OLR LOG[Power: 15S-15N]
(e)CFSv2_ann_OLR LOG[Power: 15S-15N]
(f)CFSmcm_ann_OLR LOG[Power: 15S-15N]
Anti-Symmetric/Background
n=0 EIG
MRG

Figure 4.

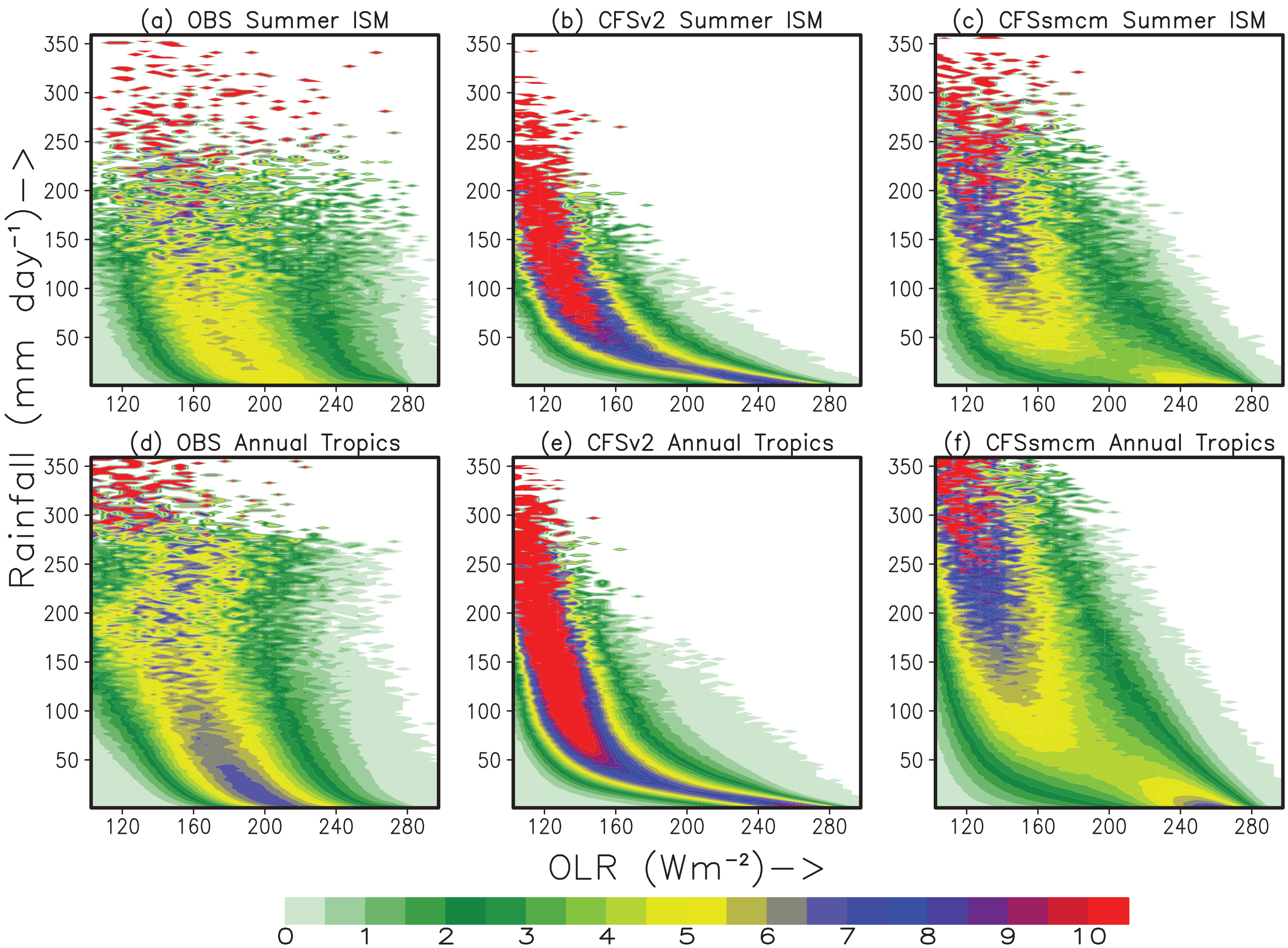
(a) OBS Summer ISM
(b) CFSv2 Summer ISM
(c) CFSsmcm Summer ISM
(d) OBS Annual Tropics
(e) CFSv2 Annual Tropics
(f) CFSsmcm Annual Tropics
Rainfall (mm day⁻¹)—>
OLR (Wm⁻²)—>
350
300
250
200
150
100
50
120
160
200
240
280
0
1
2
3
4
5
6
7
8
9
10

Figure 5.

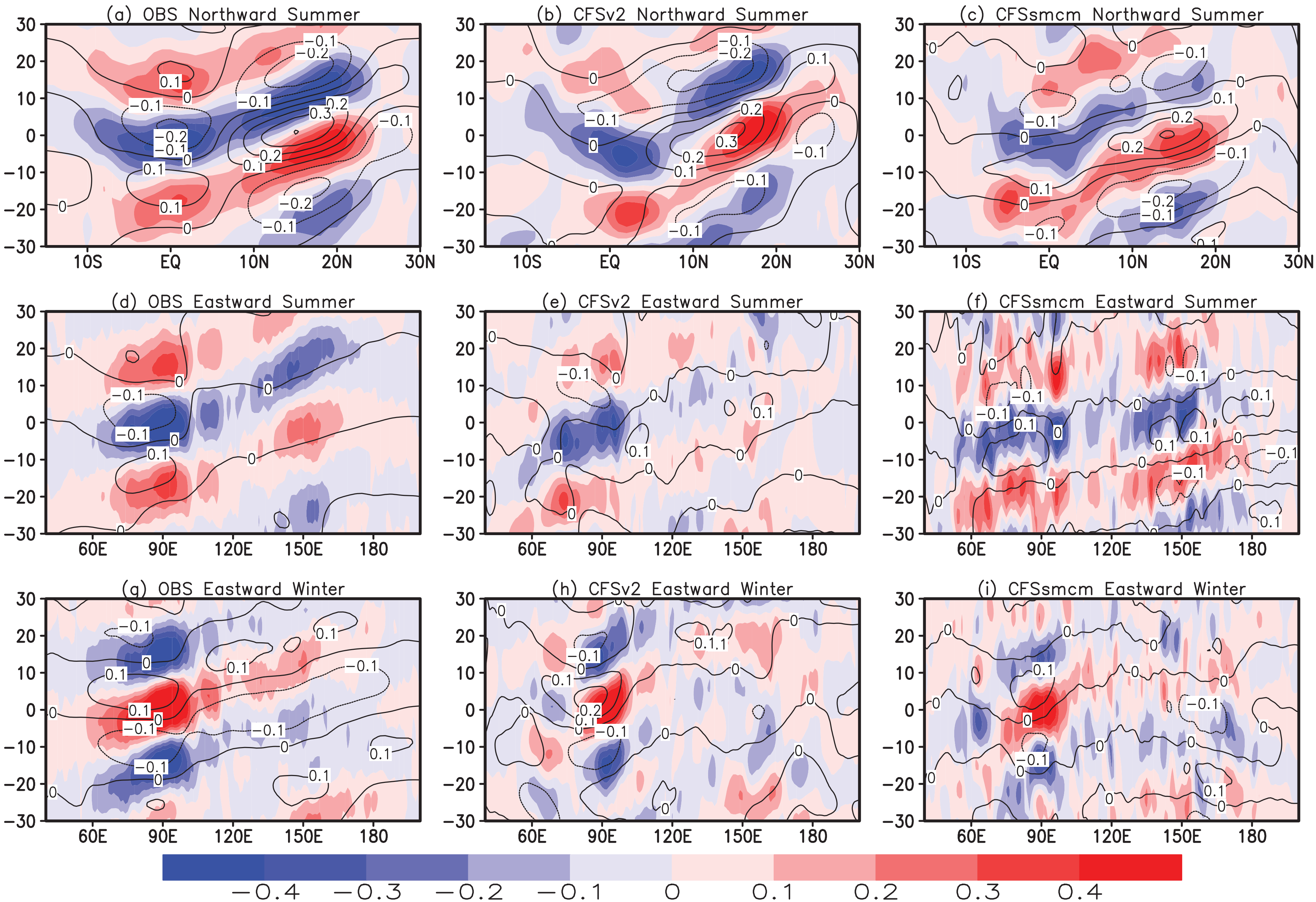

(a) OBS Northward Summer
(b) CFSv2 Northward Summer
(c) CFSsmcm Northward Summer
(d) OBS Eastward Summer
(e) CFSv2 Eastward Summer
(f) CFSsmcm Eastward Summer
(g) OBS Eastward Winter
(h) CFSv2 Eastward Winter
(i) CFSsmcm Eastward Winter
−0.4 −0.3 −0.2 −0.1 0 0.1 0.2 0.3 0.4